remote sensing

MDPI

Article

Automated 3D Modeling vs. Manual Methods: A Comparative Study on Historic Timber Tower Structure Assessment

Taşkın Özkan [1,*], Iosif Lavric [2], Georg Hochreiner [3], Norbert Pfeifer [1]

[1] Department of Geodesy and Geoinformation, Vienna University of Technology, Wiedner Hauptstraße 8/E120, 1040 Vienna, Austria; norbert.pfeifer@tuwien.ac.at
[2] Department of Geodetic Engineering, Technical University of Civil Engineering of Bucharest, Bd. Lacul Tei nr. 122-124, Sector 2, 020396 Bucharest, Romania; ilvrkiosif@gmail.com
[3] Institute for Mechanics of Materials and Structures, Vienna University of Technology, Karlsplatz 13/202, 1040 Vienna, Austria; georg.hochreiner@tuwien.ac.at
* Correspondence: taskin.oezkan@tuwien.ac.at

Abstract: The present study focuses on the preservation of historic timber constructions, crucial cultural heritage assets that demand effective structural health monitoring (SHM) to ensure safety and integrity. SHM aims to detect and evaluate potential structural deviations that may compromise performance, requiring both detailed geometric data acquisition and 3D modeling. For this purpose, contactless tools such as photogrammetry, laser scanning, and other topographic methods are employed to gather point cloud data. This research utilizes a terrestrial laser scanner (TLS) to generate 3D models of the historic timber tower of St. Michaeler church in Vienna. A novel automated modeling method is compared with two manual modeling approaches. The first is a traditional as-designed structural model created in Dlubal RSTAB software, and the second is a manually generated as-built model created using a scan-to-BIM application in Revit. While the first model is based on 2D plan documents created from the TLS point cloud, the second and automated models use the point cloud as direct input. The findings demonstrate that this automated model significantly enhances early-stage structural assessment efficiency, providing reliable insights into structural conditions with minimal processing time. This research underscores the potential of automated 3D modeling in preliminary structural assessments of historic timber structures.

Keywords: historic timber towers; 3D reconstruction; point clouds; structural assessment

Academic Editors: Devrim Akca and Massimiliano Pepe

Received: 29 November 2024
Revised: 16 January 2025
Accepted: 25 January 2025
Published: 28 January 2025

Citation: Özkan, T.; Lavric, I.; Hochreiner, G.; Pfeifer, N. Automated 3D Modeling vs. Manual Methods: A Comparative Study on Historic Timber Tower Structure Assessment. *Remote Sens.* **2025**, *17*, 448. https://doi.org/10.3390/rs17030448

1. Introduction

Historic timber constructions are significant cultural heritage assets that require proper preservation. The implementation of structural health monitoring (SHM) is a crucial aspect of the preservation of cultural heritage, ensuring the safety of these structures and maintaining their structural integrity. The main objective of SHM is to assess the potential for deviations from the intended performance of a structure due to various phenomena. This involves the analysis of the forces that act on the structure and the evaluation of their impact on its behavior [1]. Recent scientific research, [1–6], has focused extensively on examining timber structures from a structural engineering perspective. Specifically, standards and guidelines for the assessment of historic wood structures are the subject of these studies. In terms of guidelines, the initial steps for structural analysis are the acquisition of the geometry and the 3D geometrical and structural modeling of the structure. A comprehensive analysis of a timber structure would benefit from additional visual

inspection of cracks, decay, and missing connections; measurement of moisture content; and estimation of the types of materials. In this context, the present study addresses the 3D structural modeling stage of the aforementioned guidelines.

In the field of cultural heritage, contactless tools are often employed to accurately and rapidly obtain the geometry of historic structures. The more frequently used methods are photogrammetry, laser scanners, and other topographic methods (e.g., total station) [6]. The results of geometric surveys, typically point clouds, can be utilized, on the one hand, to generate 3D models in building information management (BIM) software [7] and, on the other hand, to supply data for structural analysis [8,9]. The models can also be used for virtual reality (VR) and virtual tourism [10]. In this study, a terrestrial laser scanner (TLS) [11] was utilized to acquire geometric data about the historic timber bell tower structure of St. Michaeler church in Vienna.

The structural assessment calculation begins with generating a numerical three-dimensional model through the utilization of geometrical survey data. These models encapsulate the roof's original structural design and any subsequent modifications or enhancements. This methodology facilitates the assessment of the structural condition over varying periods. Furthermore, the structural assessment calculation serves as an efficacious instrument for the evaluation of intermediate stages of assembly during the construction process [4].

The objective of this study is to illustrate the potential of automated 3D models for preliminary structural assessment of historic timber tower structures. Three distinct methodologies were employed to generate the basics of the structural models from the TLS point cloud. The first model, which refers to the as-designed model, was developed using Dlubal RSTAB v.8.28 [12] structural engineering software. Before the development of the 3D structural model, 2D maps were created using planar sections of the point cloud, which document the dimensions of the beams, the basic connections between structural elements, and the material conditions. The second model, the manually generated as-built model, was created using a Scan-to-BIM application with Revit v.25.0.2 [13], a widely used software for BIM modeling in the architecture, engineering, and construction (AEC) industry [14]. The collected point cloud serves as the direct input for this modeling method. The third method, which constitutes the primary contribution of this paper, offers an automated as-built 3D structural modeling process from the point cloud. A secondary contribution of this paper is the comparison of these three methods. The achieved level of automation produced a structural model for a historic timber tower, requiring minimal manual input. The results section shows that this automated model enables rapid early-stage structural assessment scanning with minimal processing time.

2. Related Work

2.1. Assessment of Historic Timber Structures

The examination and reinforcement of historic timber structures has been the subject of numerous scientific studies [15–27]. The relevant standards, IS0-13822:2010 [28], EN 16096 [29], and EN 17121:2019 [30], provide the general requirements and procedures for the assessment of existing structures (buildings, bridges, industrial structures, etc.) based on the principles of structural reliability and consequences of failure. Perreia et al. (2020) [5] conducted an analysis of papers and articles that focused on the assessment process of heritage, traditional, and engineered timber buildings. This analysis identified six steps involved in assessing and retrofitting existing timber structures: a desk survey (a), a preliminary survey (b), a decay and check survey (c), a structural analysis (d), a review of special requirements (e), and the design of interventions (f). Santos et al. (2023) [6] presented a review paper that summarizes existing research on historical timber structures

using historic building information modeling (HBIM) [7]. It focuses on various geometric surveying and 3D modeling methods, as well as non-geometric information included in the model, particularly related to conservation, testing, and monitoring. Additionally, the review highlights the increased effectiveness of structural health assessment when the structural analysis is implemented within an HBIM-based framework. The above studies are mostly based on roof structures. Nevertheless, the structural analysis of historic timber bell tower structures presents distinctive challenges due to the unique characteristics inherent to such structures. For example, in addition to the static structural and architectural objects, they may also hold the dynamic loading of the swinging bells.

Niederwanger (1997) [31] highlighted that for structural repair of bell towers, measuring the dynamic behavior and conducting numerical simulations are crucial. Thus, by creating a numerical model based on measured data and performing estimation of the dynamic loading of the tower by swinging bells, the best repair method can be determined. André et al. (2003) [32] employed a combination of field measurements and numerical methods to assess the mechanical properties of a wooden bell tower. It was observed that when bells are ringing, the entire wooden structure undergoes significant displacement, resulting in contact with the masonry. The structural analysis revealed that the timber components exert no influence on the system behavior, which is predominantly determined by the properties of the connections. Ivorra et al. (2006) [33] analyzed three swinging bell systems and compared the maximum values of the horizontal and vertical forces acting on the structure, as well as their main harmonics. Selvaggi et al. (2019) [34] presented an approach to deriving a finite element (FE) volumetric voxel model, of a bell tower through a semi-automatic process utilizing laser scanning point clouds. Quattrini et al. (2019) [35] proposed a methodology for transforming TLS point clouds into a 3D finite element model (FEM) in a semi-automatic manner. Given the complex nature of a bell tower, it was not feasible to divide it into discrete elements and assign distinct materials to each. Consequently, A second FEA model was generated for concrete slabs and beams, providing more results. In the study of Ghini et al. (2024) [36], a practical approach was presented to demonstrate the effects of the bell-swinging system on a masonry tower. The process entails the extraction of equivalent displacement fields that correspond to the peak displacement responses from the displacement time histories, utilizing FEM. Existing literature highlights the ongoing need for comprehensive structural analysis of heritage towers by combining accurate surveying with 3D modeling techniques.

2.2. Data Acquisition and Processing

In addition to the collection of historical documents related to the structure, the collection of geometric data represents a preliminary step before the identification of the structural situation of a heritage structure. Grussenmeyer et al. (2008) [37] conducted a comparative analysis of three data recording methods, namely TLS, photogrammetry, and tacheometry, to assess their suitability for use in the documentation of cultural heritage buildings. The results demonstrated minimal discrepancies in the deviations between the models. It can therefore be concluded that laser scanning or photogrammetry techniques can be applied equivalently, at least for flat and regular-shaped objects. In contrast to the documentation of the castle facades, timber structures frequently exhibit complex and highly irregular geometric characteristics, which makes the use of TLS a more desirable option. Wang et al. (2020) [38] discussed the evolution of light detection and ranging (LiDAR) technology, key enterprises, and their representative products. The utilization of TLS using LiDAR technology results in the generation of millions of high-precision surveyed points within several seconds, collectively referred to as a point cloud. This data can be interacted with computer-aided design (CAD) or BIM software, facilitating the

generation of numeric models. Prati et al. (2019) [39] also identified several limitations of TLS, including the cost, the need for expertise to operate, and the necessity for post-processing steps. Additionally, there is a lack of data regarding hidden spatial structures.

Point clouds contain much more information than is necessary for 3D modeling. There is a need to consolidate methodologies for post-processing point clouds, reducing the time and manual effort required for discretization, classification, and data analysis [40]. Yang et al. (2023) [41] discussed various point cloud semantic segmentation algorithms, including region growing, model fitting, unsupervised clustering, supervised machine learning, and deep learning, highlighting their advantages, disadvantages, and specific applications in cultural heritage. Musicco et al. (2024) [42] presented a semi-automatic methodology using RANSAC and Random Forest algorithms for point cloud segmentation and classification to isolate architectural elements like walls, vaults, corbels, and rafters. Segments were processed using Visual Programming Language for better accuracy and efficiency in the HBIM framework. Caciora et al. (2024) [43] propose a semi-automatic pipeline for the detection of degraded areas from point clouds of cultural heritage sites. The methodology proved to be practical and cost-effective for heritage monitoring.

2.3. Automation in 3D Modeling

The manual modeling of each member in a complex structure can require several months, and automated models may exhibit incomplete or absent beams due to process-based or data-driven occlusion. Prati et al. [39] presented a paper that primarily addresses the conversion of a point cloud into three-dimensional models through the use of parametric modeling tools, such as Grasshopper [44], and generative algorithms. The algorithms are created for a single truss. In a further contribution to this field, Massafra et al. (2020) [9] once created a single truss of the roofing system of the Municipal Theater of Bologna; then the parametric algorithms permitted the generation of 3D models of all the trusses, with modifications limited to the TLS input point cloud. In the context of the automation of the modeling process for an entire structure, Yang et al. (2018) [45] developed an API for Revit to accelerate the construction of rectangular beam geometries using total station data. Pöchtrager et al. (2018) [46] concentrated their efforts on beams with rectangular cross-sections. They employed a three-step process: first, they segmented the point cloud and then matched the orthogonal or parallel side surfaces of the beams. Finally, they fit cuboids to the corresponding segments. To increase the number of the automatically generated beams, Murtiyoso and Grussenmeyer (2020) [47] employed the Hough transform to divide complex facets into linear components; however, their approach was constrained to L- and Y-shaped segments. Özkan et al. (2022) [48] presented methodologies for the filtering of the roof cover from input data and the subdivision of complex point cloud segments into linear sub-segments, thereby increasing the number of automatically modeled beams in a timber roof structure. Özkan et al. (2022) [49] refined incomplete rafter beams in automated 3D roof models, with a particular focus on beams connected to roof tile planes. Selman et al. (2022) [50] put forth an automated methodology analogous to Özkan et al. (2022) [48], whereby the geometry and connectivity of beams are computed directly from point clouds for structural analysis. However, this approach does not include roof cover filtering and incorporates an interactive editing interface to address the issue of missing cuboid intersections, thereby facilitating the generation of suitable structural models. Özkan et al. (2024) [51] proposed a workflow that involves the automated extraction of sub-structures, such as truss systems and bracing systems, from automatically modeled beams analyzing their repetitive layout. Subsequently, a refinement process was implemented to enhance the overall structure's completeness while reducing the reliance on manual operations. The workflow was employed to conduct preliminary structural analysis under dead-load

conditions on two historic roof structures. In this study, the approach is conducted with some adaptations, which are explained in the Method section for the analysis of the tower structure.

In conclusion, TLS represents a well-established methodology for the acquisition of historic structure geometry. However, the generation of models for structural analysis remains a significant challenge, particularly in the case of complex structures. As shown in the results section, standard structural or architectural design software involves labor-intensive and time-consuming work to generate a complete model of the structure, including geometric specifications of each beam. Our contribution involves the re-implementation of the recent roof structure modeling automation methodology [51], including some adaptations to apply to the tower structure. The comparison of the as-designed models shows that around two-thirds of the processing time can be handled by the automated workflow. This paper also presents limitations and assesses the impact of imperfect automated modeling on the structural analysis.

3. Materials and Methods

3.1. Study Site and Data

The historic timber bell tower of St. Michael Church in the centre of Vienna, shown in Figure 1, is the subject of this study. Construction of the Church began around 1221 as a Romanesque–Gothic basilica, and a tower was added in stages from 1300. Fires in 1276, 1326, and 1350 caused considerable damage and delayed construction, but the tower was completed around 1400 to a height of 56–58 m. A fire in 1525 damaged the church and tower but left the structure intact, leading to repairs and the addition of a fire watch room and a new bell in 1526. An earthquake in 1590 destroyed the spire and pinnacles, prompting restoration and the addition of two levels, culminating in the current copper-clad spire, which reaches nearly 80 m. The west front of the tower was redesigned with a portico in 1724 and rebuilt in 1791. The tower has remained largely unchanged, apart from repairs to the parapet in 1955 and 2018 [52].

Figure 1. Aerial map view provided by city of Vienna (https://data.wien.gv.at, accessed on 27 January 2025) (**left**) and an image of St. Michael Church (**right**).

The motivation for creating a structural model was the urgent need for decision-making if the wooden roof structure of the bell tower was prone to collapse in terms of global rocking, although it was installed 400 years ago and performed without significant changes until today without problems. Furthermore, a concept for strengthening with modern elements made of steel, being in conflict with the historical monument, was presented without any backup by structural assessment based on appropriate documentation of the structure before.

A pilot project was agreed upon and also supported by the Federal Monuments Authority of Austria [53] in terms of funding, to leave the track of traditional procedures only based on the "experience of carpenters" and start a more professional track based on previous comprehensive documentation of the structure and subsequent structural analysis. The result should reveal if the reinforcements were necessary at all and what would be a more decent type of realization following the rules for professional monument conservation. Section 3.2.1 directly refers to the applied methodology during the project. The second and third methods, which are outlined in the Method section, represent alternative approaches that are designed to reduce the time required for data collection and subsequent handling of the 3D structural model.

For the geometric data acquisition, a survey with a VZ-400i TLS by Riegl, Horn, Austria [54] was conducted by the partner engineering office [55] of the aforementioned project. More than 70 scan positions were used. The spacing between sequential scans was 2–3 m. The Laser Pulse Repetition Rate (PRR) of the device ranges from 100 kHz to 1200 kHz, allowing for the measurement of up to 500,000 points per second using near-infrared laser beams. The device's 3D positional accuracy is specified as 3 mm at 50 m and 5 mm at 100 m. For this study, the PRR was configured to its maximum value of 1200 kHz.

Following the surveying, the collected point clouds from different scan positions were combined into a subsampled point cloud. The point cloud was exported to LAS [56] format using RiScanPro v.2.15 software [57] as presented in Figure 2. The OPALS v.2.6.0 [58] software is used to apply the point cloud processing operations. Its data format, the OPALS Data Manager (ODM), consists of two different spatial indices that allow efficient access to point attribute information. ODM organizes the point cloud into tiles (level 0 index) and dynamically constructs a k-d tree (level 1 index) for the points within a tile on access.

3.2. Method

Figure 2 illustrates the primary configuration of this study. As is standard practice, the documentation of the geometries starts with the surveying of the relevant area, which in this case involves the use of 3D scanning technology. The point cloud of the structure, obtained through the acquisition of data from multiple scan positions, serves as the foundation for the generation of a 3D structural model. This study presents three distinct modeling approaches. The first method was utilized as part of the aforementioned project, whereas the second and third methodologies were employed after the completion of the project.

Section 3.2.1 employs the use of CAD functionality of structural engineering software, specifically Dlubal RSTAB v.8.28 [12], to facilitate the creation of structural members, including nodes, materials, cross-sections, beams, and connections. In this process, the essential input is not the point cloud itself, but rather the 2D plans extracted from it. Section 3.2.2 is based on beam modeling using Autodesk Revit v.25.0.2 [13] in conjunction with the point cloud. This method exemplifies the prevalent Scan-to-BIM concept in the AEC industry. The Section 3.2.3 entails the integration of the methodologies elucidated in [51] to facilitate the automated processing of the point cloud, ultimately generating 3D structural models. This approach combines the automated derivation of beams with manual beam modeling, ensuring the structural connectivity of the model.

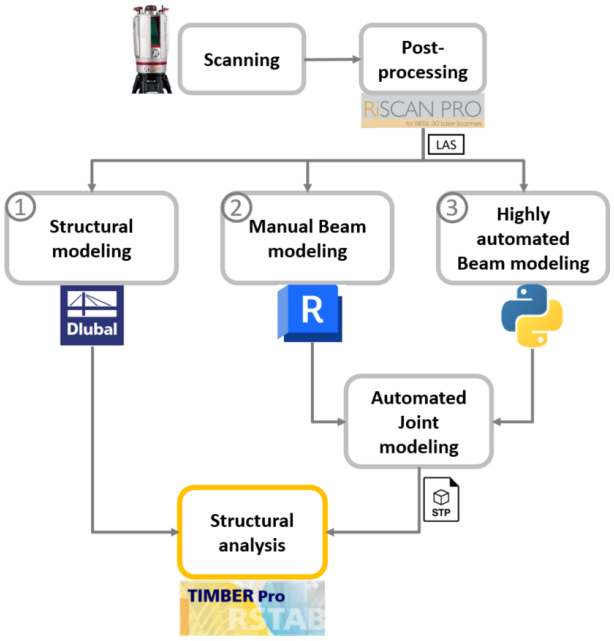

Figure 2. Main workflow of the study starting from scanning the tower, 3D structural modeling using different methods, and the preliminary structural analysis.

The first model indicates very detailed modeling of the beams and connections. In contrast, the second and third models adopt an automated joint modeling approach, as described in [48,51]. Thus, all elements are linked together to form a working system. For the comparison and structural analysis of these models, the STEP data exchange file format [59] is employed to interact with the structural engineering software.

3.2.1. Three-dimensional Structural Modeling Using Plan Documents

The first method is characterized by the following stages:

- 2D documentation of the existing situation of the structure. The proposed methodology entails the utilization of layers for data organization to facilitate the representation of horizontal planes with beams that are stacked across multiple planes.
- Generation of a structural model with initial perfect geometry, excluding any deformations. The utilization of functions such as copy and rotate is employed for simplification and efficiency.
- The addition of specifications for the beam ends in terms of correct settings for hinges, which were not subjected to manual inspection following the laser scan, is also required.

In Figure 3, a horizontal and vertical slice of 2D plans and the corresponding structural models are demonstrated. Although the engineering office in charge was equipped with devices for 3D laser scanning, the results from manual extraction—similar to the second method (Section 3.2.2)—were only documented in terms of 2D plans, representing clipping planes in horizontal and vertical directions. Following the concepts in traditional standardization of documentation of monument assessment and conservation in Austria, the minimum compromise for beams horizontally allocated in several planes was to assign each plane to a specific layer in the drawings. The typology of the connections was not included in the 2D maps, although this type of information was acquired on-site and is indispensable for the correct setting of hinge specifications in the stage of the subsequent structural modeling and assessment. The period of the manual derivation of 2D plans was not performed in one step and lasted about seven months.

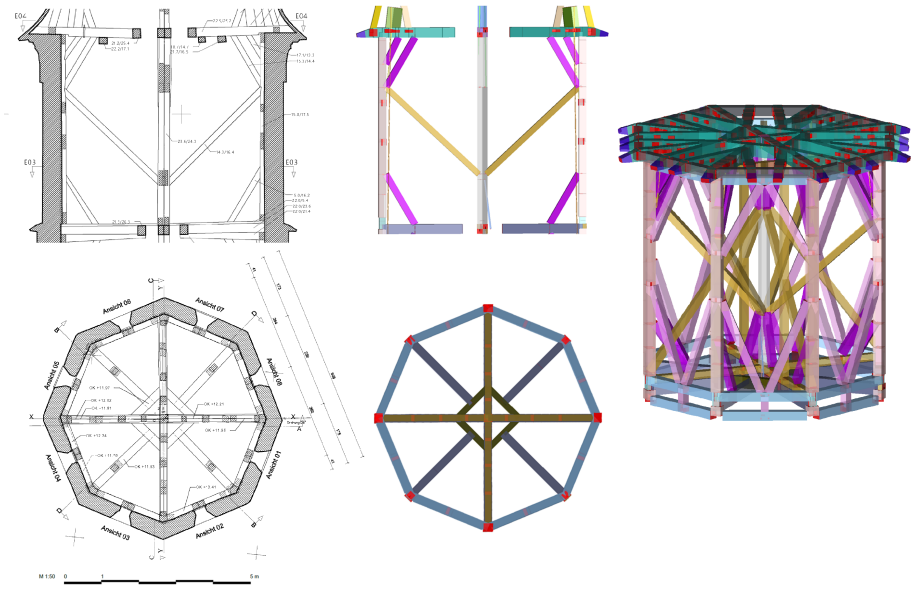

Figure 3. Two-dimensional plan examples and the structural model of the third storey. The first column illustrates the 2D plans of vertical (**top**) and horizontal (**bottom**) slices. The second column shows the modeled beams colorized by the cross-sections. On the right side, a 3D view of the storey is shown. The source of the 2D plans is "Parish of St. Michael Vienna [52], EKG Baukultur [55]".

The starting point for structural assessment is not the deformed but the initial and therefore stressless geometry at the stage of production and implementation. Following, the deformed geometry is the compilation of the initial geometry and calculated subsequent deformations. Before the background of time pressure and in conflict with numerous small geometrical irregularities, the pdf plans have been manually enriched by selected dimensions created by measurements to be used for subsequent geometrical modeling in the structural engineering software RFEM (Dlubal RFEM v.5.35). The use of CAD features like copy and rotate simplified the process of geometrical implementations, still without geometrical imperfections. Missing elements have been deleted afterward on demand. It can be assumed that the original structure has also been produced according to the master planes in perfect vertical and horizontal directions, respectively, of the whole structure. Several subsequent personal inspections on site completed the knowledge concerning the true end faces of beam elements and the typology of the connections. Due to numerous maintenance repairs and therefore induced variations of local stiffness of structural components in the past, the overall structural performance was no longer symmetric despite the symmetric concept of the structure.

3.2.2. Manual Beam Modeling from Point Clouds Using REVIT

The generation of the 3D Revit model commenced with the acquisition of a point cloud compatible with Revit v.25.0.2 software. To achieve this, Autodesk's Recap Pro v.25.0.204 [60] software was employed to transform from the LAS to the RCP format for seamless integration of the point cloud in Revit v.25.0.2.

The preliminary phase entailed the creation of a new project utilizing a metric template. Subsequently, the point cloud was imported, ensuring that "By shared coordinates", the imported point cloud retained the same coordinate system as the Revit project, thus preserving spatial accuracy. Following this, the project was prepared for 3D modeling by adjusting and creating levels for each floor of the building. This structuring step was very helpful as it facilitated a more organized and efficient modeling process, enabling easier manipulation and reference of different building sections during the modeling phase.

Three-dimensional modeling of the structure used Revit's built-in tools and features for detailed and accurate modeling. Before the actual modeling, each beam was subjected to a series of measurements, taken from the point cloud at the point of insertion, to ensure the accuracy of the resulting dimensions. However, interpreting the structure just from the point cloud can be challenging, especially without any site pictures or 2D plans. The main uncertainty is to know where a beam ends when multiple beams intersect, relying only on a point cloud. All beams were assigned the material type "generic wood". This method provides a representation of the entire timber structure, accurately reflecting the true as-built conditions, thereby minimizing potential inaccuracies in comparison with the point cloud. Nevertheless, for the interpretation and finalization of the generated model, a background in structural engineering and experience with such structures is essential to evaluate the assumptions made during modeling for a feasible structural analysis.

As illustrated in Figure 4, the modeling process is based on the analysis of clipped sections of the point cloud that are close to the beam surface planes. To clip a portion from the point cloud, side sections near the surface planes are used. To insert a beam, the first step is to import an appropriate beam family. In this study, rectangular beams were defined by the measured size of the cross-sections. Then the beams were placed at their respective starting and ending points on the point cloud. Subsequently, a refinement step was undertaken following visual inspection from both top and side perspectives. The "Align", "Extend", "Trim", and "Slice" commands may be employed to adjust the position and length of the beams by the point cloud.

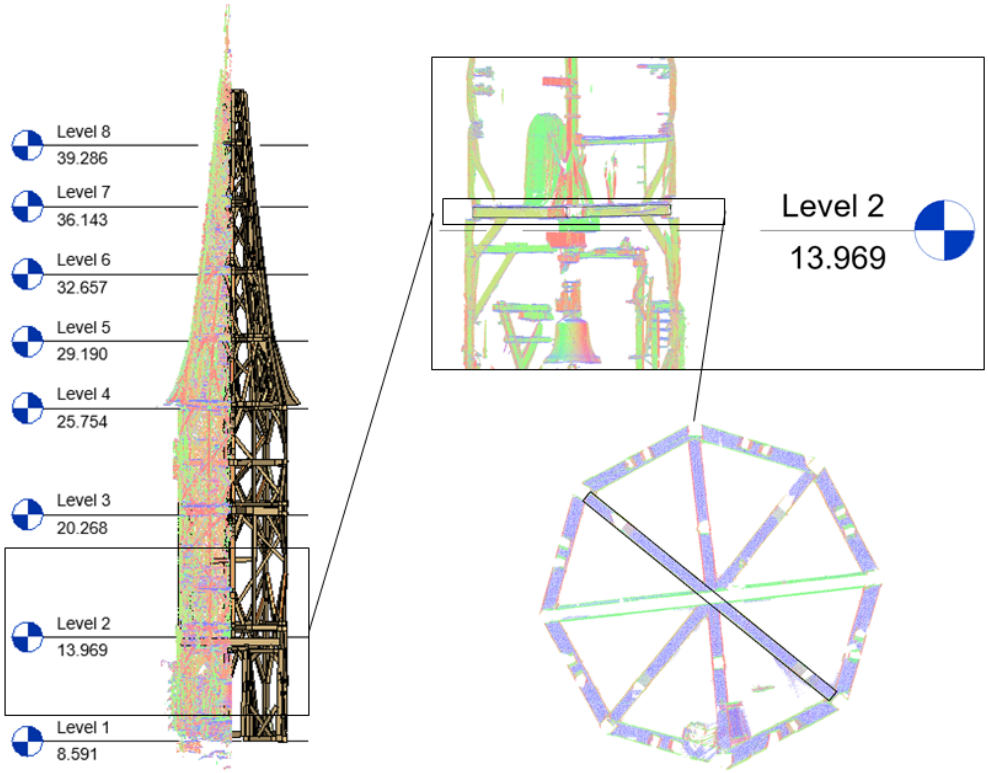

Figure 4. Manual timber beam structure modeling process in Revit v.25.0.2. Identification of horizontal levels (**left**) and cropped cross-section of point cloud on the second level for modeling of the beams (**right**).

3.2.3. Automated Beam Structure Modeling

This section highly relies on the methods presented in [48,51]. However, as these former studies were focused on historic timber roof structures, the subject of this study, a historic timber tower structure, brings adaptations to the suggested methods and work-

flows. In Figure 5, the sub-products (a, b, c, d, e) are directly generated from the point cloud using Python scripts working in an automated fashion. The final model shown in Figure 5f is a combination of the automated model (e) and manual beam modeling to ensure a complete model.

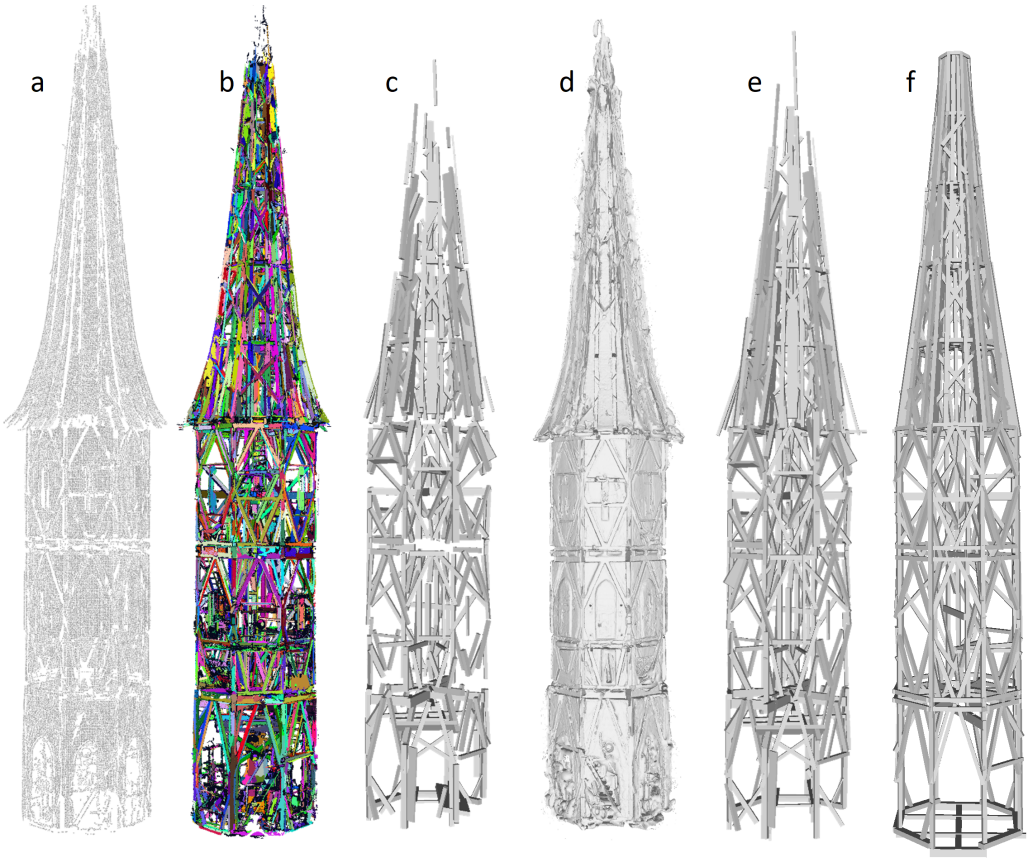

Figure 5. Processing sub-steps of the highly automated beam modeling. (**a**) coverage filtered points that serve as the input for the definition of the master planes, (**b**) segmentation of the interior points, (**c**) initial beam modeling result, (**d**) mesh model of the entire point cloud, (**e**) automatic model refinement, (**f**) final model including manually modeled beams.

For detecting and modeling individual beams, ref. [48] suggests a workflow that comprised of the following main steps: roof cover filtering to identify master planes, segmentation of the interior point cloud, classification of the segments, linear segment splitting, and cuboid modeling. In addition to the cuboids, this paper presents a methodology for modeling beams with trapezoidal cross-sections.

The first step, the coverage filtering, is based on the application of the direct visibility algorithm [61] from the surrounding six viewpoints to the point cloud. This method is applied to separately extract the outer surface and inner point cloud of the tower structure.

A region-growing [62]-based segmentation is applied on the interior point cloud using OPALS v.2.6.0 software [58]. An angle between normal vectors (α_{max}) within a search radius (r) neighborhood and a minimum number of points per segment are considered as the constraints of the segmentation (see Figure 5b). The relevant parameters are presented in Table 1.

Classification of the segments into the sub-groups named linear, non-linear, and compact is done as suggested by Pöchtrager et al. (2018) [46] using the shape factors acquired through principal component analysis (PCA) [63]. Optimally, the side surfaces of beams are represented by segments with elongated rectangle shapes. To increase the

number of linear segments, RANSAC [64] algorithm is used to split the non-linear complex segments into linear sub-segments [48] by the given parameters as described in Table 1.

Table 1. Summary of utilization of the parameters.

Processing Stage	Parameter Definition
Pre-defined parameters	w_{min} = 0.10 m, w_{max} = 0.40 m
Coverage filtering	r_1 = 0.20 m, r_2 = 0.01, $\alpha > 85^\circ$, d_{max} = 0.05 m
Segmentation	r = 0.05 m, $\alpha_{max} = 5^\circ$, min. pts. = 300
Linear segment classification	$f_{elong} > 5.0$, $f_{area} > 0.5$
Non-linear segment split	t = 0.02 m, $\alpha_{max} = 5^\circ$, $w_{min} < d_{i,j} < w_{max}$
Reference plane definition	t = 0.02 m
Beams of a reference plane	$d_{PB} < w_{max}/2$, $\alpha_{PB} \approx 90^\circ$

A cuboid is the simplest primitive object that can represent a straight or slightly bending beam with a rectangular cross-section [46,48]. To identify the side faces of a cuboid, the geometric proximity and angles between the beam side segments are used. The best-fitting cuboid can then be estimated via an optimization of 7 parameters to minimize the distance between the cuboid surface and the segment points. The parameters used for optimization are 3 angles of rotation around the main axes (X, Y, Z) of the beam, 2 shift distances from the center of gravity (CoG) of the beam along the X and Y axes, and the size of the cross-section of the beam along the X and Y axes.

Unlike previous studies [46,48,51], this study incorporates both cuboids and trapezoidal prisms to represent beams. The resulting product of beam modeling, shown in Figure 5c, is not directly applicable to the structural analysis. Even if the model provides insight into the fundamental layout of the structure, it is evident that there are still missing and incomplete beams.

Trapezoidal Prism Fitting

This section presents the methodology for the formulation of trapezoidal prism fitting on the point cloud of beams exhibiting a trapezoidal cross-section.

Regarding Figure 6, $i = (1, 2, 3, 4)$ are the numbers of the beam faces. On the left side, C_i is the center point, n_i is the normal vector, and l_i is the largest eigenvector of the side face i. In the center, the top view of a beam with a trapezoidal cross-section is illustrated. CoG is the centroid point of all points belonging to one of the side faces of the beam. s and t are the shifting distances from CoG along r_1 and r_2 directions to the local origin (P_0) of the beam. a is the width of the side face 1, and b is the distance between side face 1 and 4. θ_2 and θ_3 refer to the angles between the normal vector of face 1 and faces 2 and 3. The figure on the right side shows a trapezoidal prism with its local origin point and three orientation vectors, $r1$, $r2$, and $r3$. A plane of a beam face is formulated as $ax + by + cz + d = 0$, in which the unit normal vector refers to $n_i = (a, b, c)_i$.

For detection of the adjacent beam faces, the following conditions are checked:

- Angle between longitudinal axes close to zero:

$$l_1 \approx l_2 \approx l_3 \approx l_4$$

- Angle between normal vectors:

$$n_1 \approx n_4$$

$$\arccos(|n_1 \cdot n_2|) - 90^\circ > \delta$$

$$\arccos(|n_1 \cdot n_3|) - 90^\circ > \delta$$

- Absolute distance between the centroid of side faces ($i = 2, 3, 4$) to the plane of the front face ($i = 1$):

$$|C_2 \cdot n_1 + d_1| < w_{\max}/2$$
$$|C_3 \cdot n_1 + d_1| < w_{\max}/2$$
$$|C_4 \cdot n_1 + d_1| < w_{\max}$$

To estimate the adjacent side faces that are not orthogonal, δ is given as an inclination threshold. w_{max} is the maximum beam width constraint for spatial limitation of the neighbor beam face searching.

Within this approach, to estimate the best-fitting trapezoidal prism that fits a given beam, it is necessary to have at least one of the parallel beam faces ($i = 1$ or $i = 4$) and both of the side faces ($i = 2$ and $i = 3$) present. After that, minimizing the distance between points to their corresponding side faces, the optimized parameters can be estimated. The input for the optimization process includes 3 rotation angles (α, β, γ) around the main axes (r_1, r_2, r_3), shifting distances from the CoG (s, t), beam size (a, b), and opening angles of the side faces (θ_2, θ_3) are required. If the cross section is symmetric, only θ_2 is optimized, and θ_3 and θ_2 are assumed to be the same.

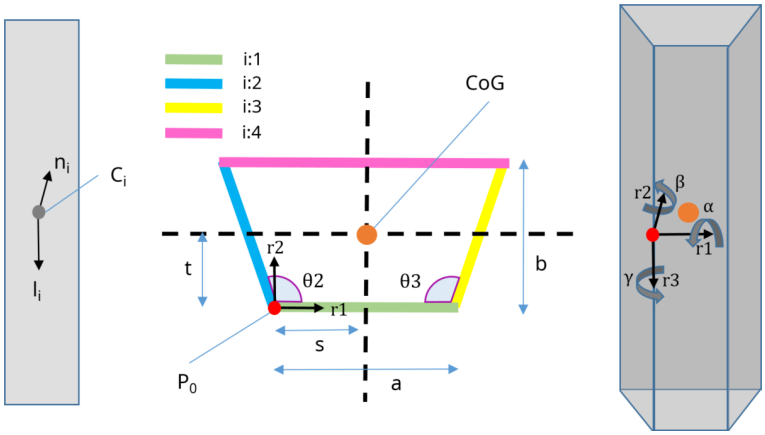

Figure 6. A beam face is represented by its minimum bounding rectangle (MBR) (**left**), a top view of the cross-section that is passing through the CoG of a trapezoidal prism (**center**), and a 3D view of the trapezoidal prism.

Equations (1) explain the definition of the plane parameters related to the input values of the optimization.

$$\begin{aligned}
P_0 &= CoG - r_1 \cdot s - r_2 \cdot t \\
n_1 &= r_2 \\
d_1 &= -P_0 \cdot n_1 \\
n_2 &= cos(\theta_2) \cdot n_1 + sin(\theta_2) \cdot (r_3 \times n_1) \\
d_2 &= -P_0 \cdot n_2 \\
n_3 &= cos(-\theta_3) \cdot n_1 + sin(-\theta_3) \cdot (r_3 \times n_1) \\
d_3 &= -(P_0 + r_1 \cdot a) \cdot n_3 \\
n_4 &= r_2 \\
d_4 &= -(P_0 + r_2 \cdot b) \cdot n_4
\end{aligned} \tag{1}$$

The sum of squared distances (SSD) of a trapezoidal prism is given by

$$\mathrm{SSD} = \sum_{i=1}^{4} \sum_{j=1}^{m} (X_{i,j} \cdot n_i + d_i)^2$$

where $X_{i,j}$ refers to the point j of the beam face $i = (1, 2, 3, 4)$, n_i and d_i represent the plane parameter of the beam face i. The minimization process of the SSD results in the best-fitting trapezoidal prism parameters. A best-fitting trapezoidal beam together with the corresponding segmented point cloud are demonstrated in Figure 7.

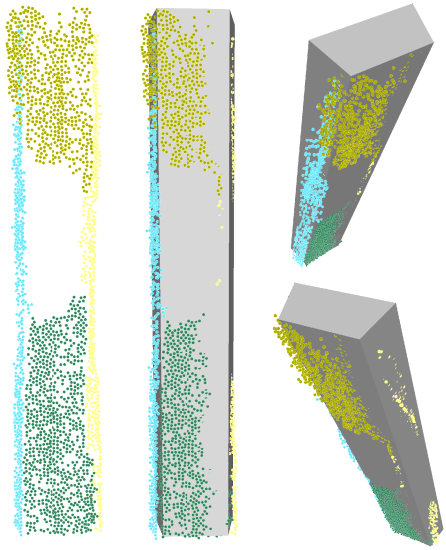

Figure 7. A trapezoidal beam with segmented point cloud. On the left, dark and light green-colored segments refer to the front face ($i = 1$), blue-colored points are the left side ($i = 2$), and yellow color shows the right side ($i = 3$). In the middle, fitting trapezoid and points are illustrated together. In the right column, points and beams are shown together from two different perspectives.

Automation Workflow and Corresponding Parameters

Concerning the tower structure, the methodology outlined in [51] is partially applicable. Before the refinement stage, it is essential to address some challenges. Firstly, the structure was designed with a vertical orientation, thereby avoiding any horizontal repetition of the sub-structures. Secondly, in this case study, the design of the structure is octagonal, comprising eight sides and eight corners around a central vertical rotation axis. Thirdly, the structure rises vertically until the third storey, at which point the vertical side beams are slightly oriented in each storey towards the central axis, thus forming the conical roof section until the top of the structure.

To generate a complete model of the tower structure in an automated manner, the workflow presented in Figure 8 is utilized. The point cloud and automatically modeled beams illustrated in Figure 5b,c are the essential inputs of the given workflow. Figure 5e refers to the result of the automated model refinement process, while the complete model is illustrated in Figure 5f.

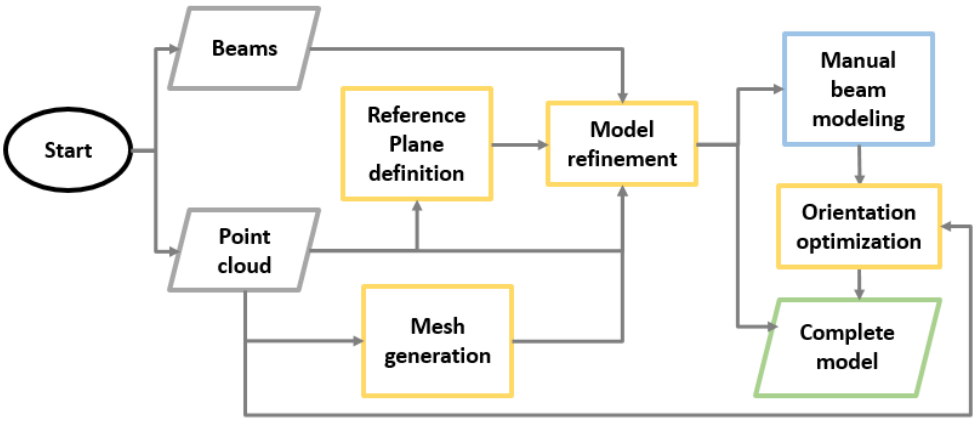

Figure 8. Workflow of the highly automated complete modeling. Grey color represents the input objects, yellow shows the automated processing steps, blue refers to the manual operation, and green shows the resulting product, a complete model that is the combination of automatically refined and manually modeled beams.

In Table 1, the parameters used in the individual steps of the workflow are presented. The parameters are explained in detail below:

- Pre-defined parameters refer to the minimum and maximum cross-section size of the beams of the structure. This information was acquired by a visual inspection of the point cloud.
- Coverage filtering: With reference to [48], r_1 and r_2 are downsampling and upsampling values, $d_{\max}$ is the thickness distance threshold to differentiate inner and coverage point clouds, and $alpha$ is the angle between the coverage surface plane and the normal vector of a neighboring point. If $alpha$ is larger than the given threshold, the point is assumed to be a member of a beam, thus the inner point cloud.
- Segmentation: r defines the value of the neighborhood search radius, $\alpha_{\max}$ is the maximum angle between normal vectors of neighbor points, and $min.pts.$ is the minimum number of points to represent a segment.
- Linear segment classification: referring to [46], $f_{\text{elong}} = \sqrt{\lambda_1/\lambda_2}$ is the elongation factor defined by the largest (λ_1) and second largest (λ_2) eigenvalues of a segment, and $f_{\text{area}} = \text{A}_\alpha/\text{A}_{\text{MBR}}$, where A_α is the area of the alpha shape of the segment and A_{MBR} is the area of the minimum bounding rectangle (MBR) of the segment.
- Non-linear segment split: as described in [48], t is the residual threshold for the line detection on 2D alpha-shape, $d_{\text{i,j}}$ is the distance between lines (i,j), and $\alpha_{\max}$ is the maximum angle between lines to detect parallel lines forming a beam.
- Reference plane definition: t is the residual threshold value of RANSAC [64], applied on the coverage point cloud.
- Beams of reference plane: as described in [51], d_{PB} is the distance between a reference plane and a beam, and α_{PB} is the angle between the longitudinal axis of the beam and the reference plane.

Reference Plane Definition

Reference planes, also known as master planes, are the basis for the comparison of point clouds and beams that are members of a planar sub-structure. Because of the different characteristics of the structure of this case study, the reference plane definition process differs from the method explained in [51]. Regarding the octagonal shape of the horizontal cross-section of the body of the entire tower structure, an RANSAC-based plane detection is applied on the covering points of the structure. Before the application of plane detection, the conic roof part is excluded from the input covering point cloud manually to simplify

the detection of eight side planes. In Figure 9, different colors represent detected eight planar point groups. The planes are formulated as $ax + by + cz + d = 0$, in which (a, b, c) indicates the normal unit vector of the segment's plane (n_S). Dashed black lines represent the 2D projections of the detected planes on the horizontal surface. In addition to the eight planes on the surface of the tower, four more planes that are passing through the CoG of the tower are defined. Firstly, the normal vector of any plane is rotated around the Z axis using the Rodrigues rotation formula [65] with the following angles: 22.5°, 67.5°, 112.5°, and 157.5°. The information on the orientation of a rotated normal vector and the position of the CoG represent the extracted central planes.

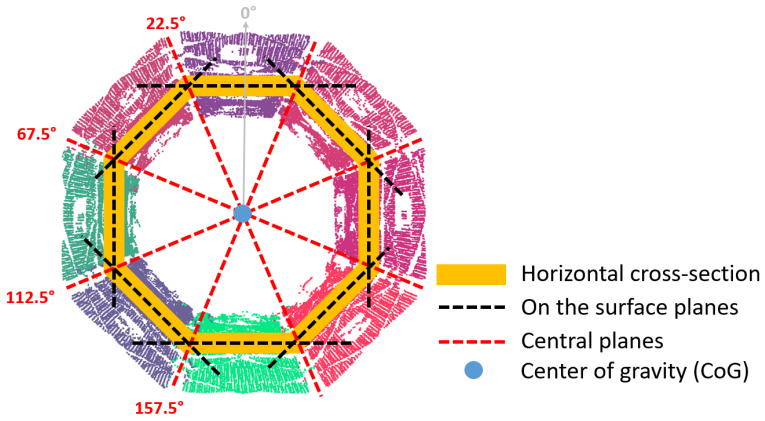

Figure 9. Top view of the segmented planes on the coverage surface of the point cloud and derived central planes.

Model Refinement

Refinement of the model concentrates on creating the missing beams that cannot be modeled, extending the beams to their full extent to fulfill the connectivity, and merging the piecewise modeled beams into single beams. The defined planes are used to apply the 2D image-processing-based approach proposed in [51]. This method is based on a comparison of the projection of the longitudinal axes of the modeled beams with the point cloud within the 3D convex hull of those beams to apply a refinement operation. Due to the intricate nature of the structure, the beam-extending decision is superseded by a 3D ray casting constrained by the mesh of the point cloud instead of 2D distance thresholds. The Poisson surface reconstruction method, as outlined by Kazhdan et al. (2006) [66], is employed to generate the mesh model shown in Figure 5d. To extend a beam, a maximum extension distance threshold is applied (the mean value of the cross-section dimensions + 30%).

Manual Beam Modeling

As illustrated in Figure 5e, the refinement stage has not resulted in the inclusion of all the required beams. To guarantee the structural integrity of the construction for a preliminary structural analysis, it is essential to create models of the missing beams. In this case study, manual modeling is conducted using the DLUBAL RSTAB v.8.28 structural engineering software. Firstly, the automated model is imported into the software using the STEP format. The creation of new beams is facilitated by the utilization of modeling operators, such as move, rotate, and mirror, which are employed to generate beams that are integrated into the existing structural layout. To facilitate comprehension of the deficiencies in the existing model, the points far from any beam surface (e.g. more than 4 cm away) are employed as a visual reference. The version of Dlubal (Rstab v.8.28) utilized in this study lacks the capacity for point cloud interaction. Consequently, the manually modeled beams' position and orientation are enhanced through the application of the iterative closest point

(ICP) algorithm, as described by Besl et al. (1992) [67], to minimize the distance between the model and the point cloud.

Automated Joint Modeling and Interoperability

A timber structure must be constituted of connected beams to ensure its structural integrity. Moreover, the juncture of intersecting beams requires the incorporation of specific mechanical characterization by degrees of freedom (DoF) within the structural model [51].

The process of automated joint modeling is comprised of two distinct stages. Firstly, the condition of the beam-to-beam intersection is identified. Secondly, the shortest line segment between the two intersected beams is determined, utilizing the longitudinal axes of the aforementioned beams, as detailed in the reference cited herein [68].

To interact with structural engineering software, the generated beams and joints need to be transferred to a proper data exchange format. The Industry Foundation Classes (IFC) constitute a set of data file formats that are used in the context of industrial automation [69]. The objective is to establish international standards for the import and export of structural objects and their properties. IFC standards may be represented in a variety of file formats, including the STEP physical file structure following ISO 10303-21:2016 [59].

A STEP format file is generated to store the structural model. The file contains the beams, with their respective starting and ending points along the longitudinal central axis, accompanied by material information (C24 softwood, as observed in the case study) and the dimensions and orientation of the cross-sections. It is assumed that all joints are rigid-to-rigid couplings, thus stored as rigid line segments within the file. While it may not be ideal to use a fixed type of connection for the entire structure, these connectors are useful for a preliminary structural analysis.

3.3. Preliminary Structural Analysis

Dlubal RSTAB v.8.28 software is employed to evaluate stress components and utilization grades based on material strength parameters as described in [51]. Following the importation of the STEP file into the software, the process begins by defining a load case along the direction of gravity, with a permanent load duration that incorporates the structure's self-weight. Then, the TimberPro module is used for a first assessment of stress components induced by internal forces from the dead load case. The calculated internal forces and global deformations for the models generated by the three different methods that were explained above are presented in the Results section.

4. Results

Referring to the three different methods that are explained in the Method section, this section provides a detailed analysis of those models. As a starting point for the surveying of the tower structure, more than seventy scan positions were conducted. The scanning campaign resulted in 1.4 billion points, which were reduced to 6.3 million points after subsampling and filtering of the coverage.

4.1. Automated Modeling

Within Section 3.2.3, segmentation of the interior point cloud resulted in 5324 segments. An amount of 418 beams shown in Figure 5c were generated through the utilization of 4212 linear segments in the beam modeling step. Following this, automatic model refinement led to the generation of 664 beams (Figure 5e). The final model, after manual beam modeling, is presented in Figure 5f and comprises 921 beams. The final model shows that 72% of the beams can automatically be modeled.

Figure 10 illustrates the projected points onto a coverage surface plane in green, while gray represents the modeled beams. Figure 10b depicts the beams before refinement, and

Figure 10c illustrates the result of the refinement. On the right side, Figure 10d illustrates the rafter structure point cloud (pink) and the beams before refinement (gray) projected onto a central plane. Figure 10e depicts the refined beams, and Figure 10f demonstrates the clustered point cloud belonging to a modeled beam (blue) and other points (red). The red clustered points will serve as a guide for manual modeling to identify the locations of the new beams. Figure 5e illustrates the outcome of the model refinement process.

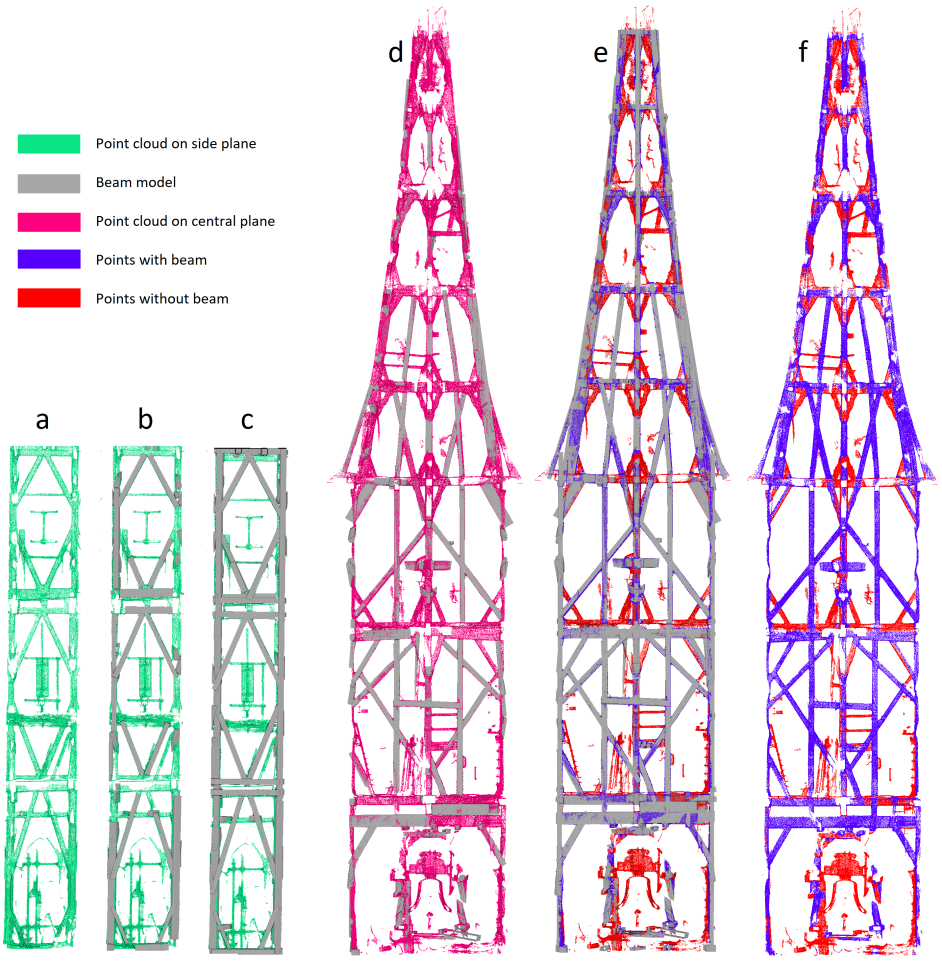

Figure 10. Model refinement based on the coverage surface reference plane (**a**–**c**) and a central reference plane (**d**–**f**).

4.2. Comparison of the Models

In Table 2, the first model is the 3D structural model of the tower, which was generated using the plan documents as explained in Section 3.2.1; the second model is the output of the method of Section 3.2.2, and the third model, which indicates the main contribution of this paper, refers to the method in Section 3.2.3. While the number of beams in models 2 and 3 are almost equal, the first model has more than two and a half times the number of beams of the other two models. One reason is the subsequent segmentation of existing beams at locations with intersections and respective connections along the beam axis, which is a matter of the engineering software. Secondly, local change in cross-sections results in individual beams along the beam axis. Further beams at the basement are also not included in 2D plans or point clouds. Furthermore, the initial model contains some connections represented not only by axes but also by cross-sections. The volume difference also highlights the effect of the additional beams in the first model. On the other hand, the small difference between the number of the beams in the last two models comes from the operator or automation decisions if the beams are partitioned or not. Additionally, while

the second model contains eight trapezoidal beams, this number was five in the automation process of the third model before manual additions. The processing time column shows the time required for the generation of 3D structural models using these different methods. To initiate the first method, a prior 2D planning documentation process, which may take several months, is necessary to complete the structure. The second model's processing time refers to the generation of the model using Revit v.25.0.2. For the third method, the estimated processing time is the combination of one hour of automated processing and an additional eight hours of manual work.

Table 2. Comparison of beam modeling results.

Model Name	Nr. Beams	Volume (m^3)	Processing Time (h)
1—Dlubal model	2621	60.35	40
2—Revit model	916	54.14	25
3—Automated model	921	52.47	9

Figure 11 and Table 3 illustrate the comparison of histograms and statistical data obtained by absolute distances between the models and the point cloud. The distances are calculated using CloudCompare v.2.11.3 [70], and the Histo module of OPALS v.2.6.0 is then used to compute the statistics and histograms. Distances greater than 3 cm are deemed irrelevant and may include elements such as floors, railings, and stairs.

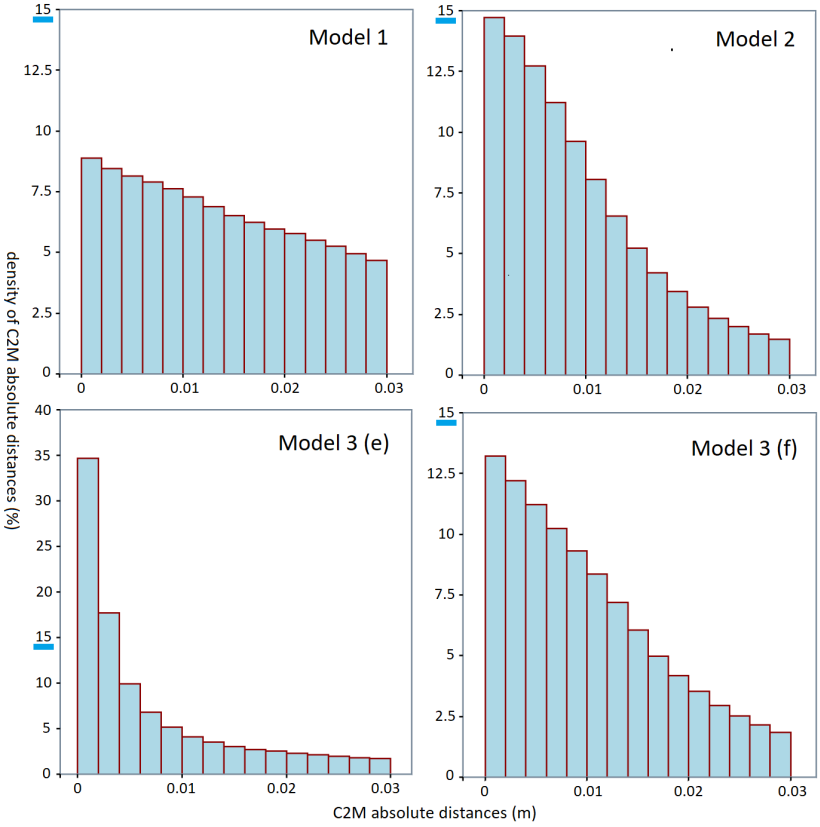

Figure 11. Histograms of the point cloud to model (C2M) absolute distances for the 3D models. The first row shows the distribution of the density of the distances of Model 1 and Model 2. In the second row, Model 3(e), the automated model, refers to Figure 5e, and Model 3(f) represents the final model (see Figure 5f) after manual additions on the automated model. Within the histograms, only the points with a maximum 3 cm distance are considered.

Table 3. Comparison of C2M statistics of the models. The statistics calculated from the distances are shown in the table in meter units.

Model Name	Nr. Pts Used	Mean	Median	Std. Dev.
1	1,859,129	0.013	0.012	0.009
2	3,207,645	0.009	0.008	0.007
3(e)	2,533,370	0.007	0.004	0.008
3(f)	3,132,181	0.010	0.009	0.008

The histogram of Model 1 visually differs from the histograms of the second and third models. The distributions on the histograms demonstrate how well a model is fitting on the point cloud. The number of used points column is also a reference that shows how the points are spatially close to the models. The number of used points and distribution of the histogram clearly show the effect of the modeling based on 2D plans in comparison with the direct point cloud-based modeling. The footprints of the histograms of Models 2 and 3(f) are very similar, indicating that they are as-designed models. Model 3(e), which was generated without any manual intervention, exhibits a more notable peak at shorter distances. Table 3 illustrates the median of the automated model, which serves to present the accuracy and robustness of the automated model in comparison with a manual model (Model 2) and the contribution of manual modeling to the automated modeling process (Model 3(f)). In summary, Model 3(f) exhibited comparable geometric precision to that observed in Model 2. Automation allows for the acquisition of an equal model with limited human interaction and in a shorter period.

In Table 2, the volume difference between Model 2 and Model 3 is 1.67 m^3. Given that the automated modeling process incorporates an optimization procedure to minimize the distances between the point cloud and the model, a minor underestimation is to be anticipated. Nevertheless, the volume difference represents 3% of the entire structure, which cannot be explained by the optimization process alone. To illustrate the differences between the two models, Model 2 is sampled as a point cloud, and then absolute distances to Model 3 are calculated using Cloud Compare. Figure 12 illustrates the sampled points colorized by distance, with green highlighting the positions of the beams that cannot be covered in Model 3. A visual inspection of Model 3 reveals that the endings are relatively short, particularly at the outset of the conical roof section (left part of Figure 12). In addition, as shown on the right side, especially in the case of stacked beams, the segmentation of the side faces and thus the fitting of the beams to the corresponding segments is error-prone. In conclusion, a user interface that allows point cloud and model interaction is crucial for finalizing an automated model, especially for the beam endings and modeling of stacked beams.

4.3. Structural Analysis

Structural analysis conducted in this study shows that the generated models can be imported and processed by structural engineering software. It must be acknowledged that the results of this analysis represent only a preliminary assessment of the models in question. There are some notable differences between the first model and the other two models. The initial model incorporates stressless and deformation-free beams, which reflect the original design concept of the structure. In contrast, the second and third models are based on the point cloud, with the beams already deformed and under stress. Secondly, the initial model demonstrates comprehensive documentation of the types of connections and materials, as well as surface objects such as concrete walls and ceilings, and well-defined supporting nodes, both on the ground and on the surrounding surfaces of each storey. Following the modeling process, nodal supports on the ground level were applied in Dlubal

RSTAB v.8.28 for the second and third models. This enabled a load analysis to be conducted, which was a crucial step in the process.

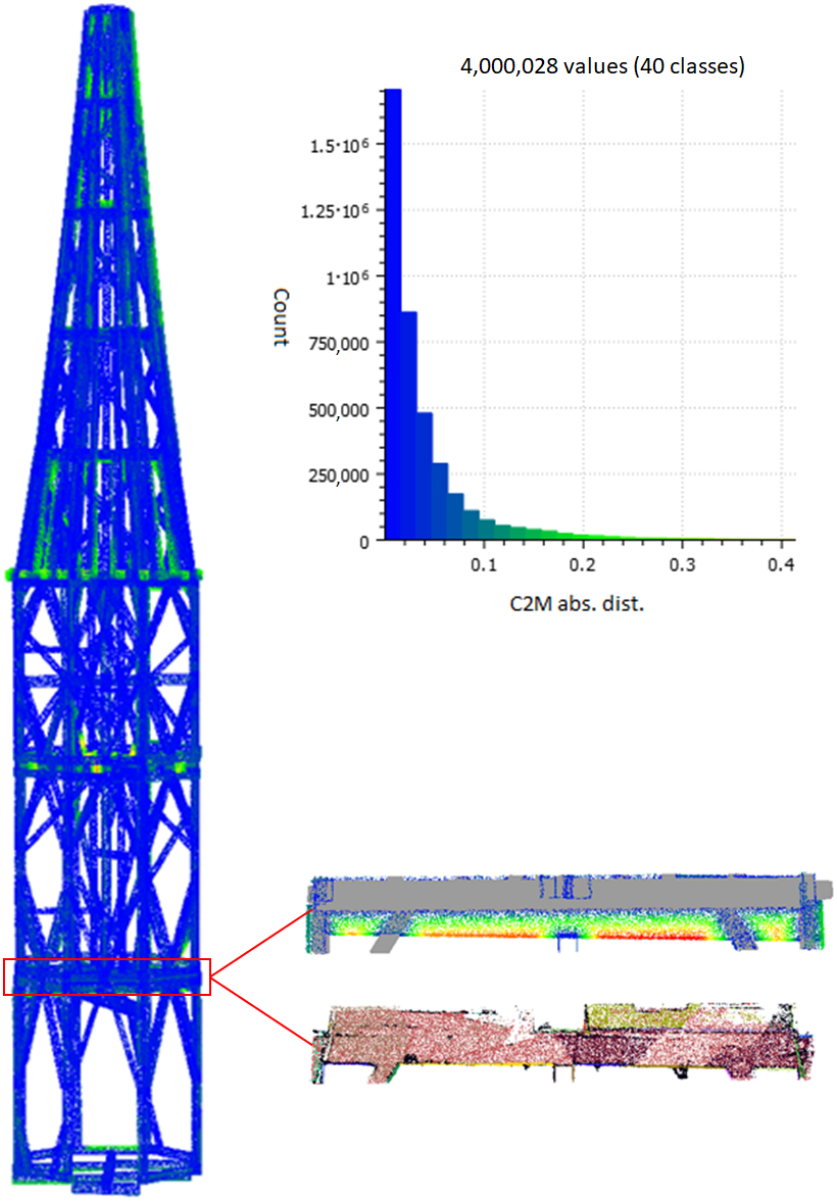

Figure 12. Comparison of absolute distances between the sampled point cloud of Model 2 and Model 3(f). Blue colors represent the closest points to the model in the left figure and the histogram. A horizontal beam, which is a stacked beam that can not be completely modeled in Model 3(f), is demonstrated in the bottom right part. The upper beam is represented by the sampled points of the Model 2 colored by distances and the beams as mesh objects in gray color. At the bottom, a segmented point cloud of the same section is displayed.

Figure 13 presents the results of the preliminary structural assessment conducted on three models. The first row of Figure 13 depicts the internal forces acting on the beams, represented with a color-coded legend. In the calculated forces, negative values indicate compression, while positive values correspond to tension in the beams. Regarding tension, the models exhibit very similar characteristics. The observed compressions are predominantly associated with the vertical long beams located at the eight corners of the tower. Since the second and third models only include supports at the ground level, higher compression effects are noted on the first storey of these models. The second row of Figure 13 shows the global deformations under the defined load condition. The effect of

further supports allocated at level 4 at the top of the surrounding stone walls is visible on the first model by the bent appearance of the scaled deformations. Similar to forces, the second and third models demonstrate similar patterns on the colorized figures. At the top of the roof part, these models clearly show the inclined situation of the structure to the left side for the shown perspective. In contrast, the initial model was modeled straight along the vertical direction, thus deformations are aligned to the direction of gravity. In summary, the initial model exhibits a maximum deformation of 1 cm, whereas the second and third models show deformations of 0.5 cm, highlighting the semi-rigid behavior of connections, which is already included in Model 1.

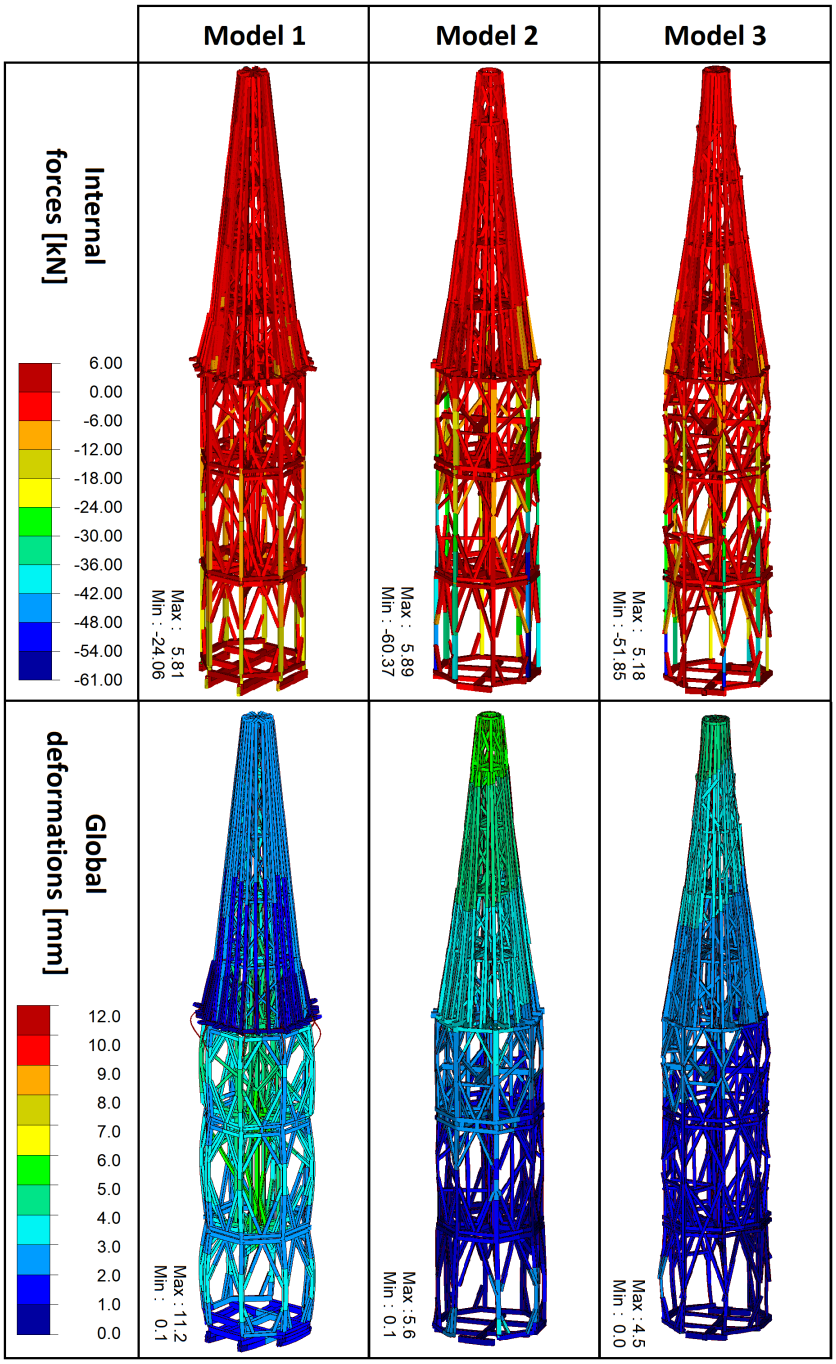

Figure 13. Preliminary structural analysis of three models under dead-load conditions. Internal forces affected by the structural elements are colorized, referring to the legend (**top**), and global deformations on the beams in mm units (**bottom**) for the generated three models. Global deformations are scaled by 100 to visually demonstrate the changes better.

5. Discussion

As presented in the related work section, using TLS enables the generation of dense and highly accurate geometric data on-site. However, the scanning process presents some specific challenges, especially with dense and narrow structures. For instance, the narrow stairways within the structure provide limited space for operators during scanning. Additionally, because of the structural diversity, numerous scanning positions are required to capture comprehensive surface data and minimize shadow effects in the resulting point cloud. Moreover, if the scanner position is unstable, inaccuracies can arise in the point cloud data, as seen in historic roof structures.

Figure 5a,b shows that the point cloud acquisition was limited by the accessibility. It was not possible to scan the uppermost stories due to solid coverings that restricted access. The survey points are limited to data collected through small openings in the wooden panels. As a result of that, the structural model needs to be completed through an expert vision. The models presented are limited by the point cloud acquisition and therefore include beam modeling up to level 8 as shown in Figure 4.

The methods presented in this study aim to generate a 3D structural model of the tower for use in structural assessment analysis. The first model, the as-designed model, represents the initial perfect geometry of the structure. This model shows the stressless and deformation-free geometric design of the structure. In contrast, the second and third models directly relied on the point cloud, which means that they represent the deformed as-built geometry. In the context of the level of detail (LOD), the initial model is designated as LOD 350, while Models 2 and 3 are identified as LOD 300 following the ISO-19650 standard [71].

Automated modeling methods show the implementation of existing state-of-the-art roof structure modeling methods with some adaptations. The first adaptation is the inclusion of trapezoids in addition to rectangular cross-sections for beam modeling. The second adaptation relates to the definition of the master plane to improve the completeness of the automatically generated beams. Due to the narrow nature of the conical roof part, the noise level on the point cloud, and the rigid obstacles covering the ceiling, the definition of master planes and thus the application of model refinement was not feasible for the roof part. Therefore, only 12 master planes (8 on the sides plus 4 through the center) were considered for the refinement stage. The final adaptation was the use of 3D ray casting instead of 2D image processing-based ray extension, which helps to reduce the over-extensions caused by 2D projection. Compared with the roof structures, the level of achieved automation decreases from 98% (as achieved in [51]) to 72%, primarily due to the difficulty in defining master planes and their relationship to the beams.

For the application of the loads on the structural model, the usual case is to use an as-designed model to observe the affected deformation, compression, stress, etc. On the other hand, even if as-built models already include the deformed geometries, these models are still valid for a preliminary structural load analysis as demonstrated in Figure 13. The initial model can be generated directly from the as-built model using a conversion algorithm such as that used in [9]. In addition to the beams, the joints and supporting objects are also essential inputs to apply the load analysis. Model 1, the initial model, indicates the presence of various types of joints and support objects, including lines and surfaces, as observed on the site. In contrast, Models 2 and 3 have only rigid-to-rigid connectors between connected beams, which are suitable for a preliminary structural analysis. Moreover, Models 2 and 3 are supported only by nodal structures on the ground. The initial model is supported by lateral surfaces, which have been needed for the generation of wind loads by computational fluid dynamics (CFD), and nodal supports on the ground base and level 4. Although this

paper does not focus on joint type detection, the lack of a clear definition of the appropriate joint types represents an incomplete step in the automation approach to structural analysis.

6. Conclusions

Three distinct structural models of a historic tower structure were independently generated through the utilization of a TLS point cloud. The models address the conversion of point cloud data into elements of a structural model as comprehensively as possible. Missing details, such as beam end connections that are not detectable using point cloud data, are to be assessed on site. The initial model includes specifications for hinges, supports, and load scenarios. The second model includes the entire layout of the beams with their cross-sections, orientations, and lengths. Interaction between the point cloud and the model via the user interface allows the beams and points to be viewed from different perspectives, providing a better understanding of beam orientation, and size estimation becomes possible. In comparison with using the 2D plans, this approach results in more accurate geometric representation within a comparatively short time. The third model, which was generated through an automated process, is capable of producing results that are comparable to those of the second model in a remarkably short time frame. As the missing beams were modeled manually after automated modeling, the analysis presented in the results section demonstrates the importance of an interactive user interface for manual beam modeling.

In conclusion, an automated model, which contains 72% of the entire structure in this case study, can be the starting point for the beam modeling process. This model can be used as a preliminary reference, providing not only existing beam data but also a list of cross-sections for the creation of any missing beams. Having a list of existing cross-sections also addresses a time-consuming part of the second modeling approach. Nevertheless, the user interface guidance employed in the second model is of significant importance in the creation of the final model, which should be as comprehensive as possible and include stacked beams and correctly estimated beam endings.

The current automated beam modeling method can model straight beams with rectangular or trapezoidal cross-sections. This study also demonstrates that the recently developed methods for roof structures with rectangular ground floors explained in [51] can be used for tower structures with the explained adaptations in the method section. Further enhancements to the automated modeling process can be made for initially curved beams and different cross-section types. Additionally, since the current method can generate the majority of beams in a fully automated manner, it has the potential to be integrated with machine learning techniques, including generative artificial intelligence, to further enhance the level of automation. Furthermore, the automated beam modeling approach can serve as a basis for generating an initial model with the guidance of master planes that are already extracted during the automation process. The results demonstrate clearly that the current methodology facilitates the accelerated, accurate, and robust modeling of beam geometries. However, generating an initial model still requires a detailed inspection of the beams' condition, connection types, materials used, and other structural elements.

Author Contributions: Conceptualization, T.Ö., G.H. and N.P.; methodology, T.Ö., I.L. and G.H.; software, T.Ö.; validation, T.Ö. and G.H.; formal analysis, T.Ö. and G.H.; investigation, T.Ö.; resources, T.Ö., I.L. and G.H.; data curation, T.Ö.; writing—original draft preparation, T.Ö.; writing—review and editing, T.Ö., I.L., G.H. and N.P.; visualization, T.Ö. and I.L.; supervision, G.H. and N.P.; project administration, N.P.; funding acquisition, N.P. All authors have read and agreed to the published version of the manuscript.

Funding: This research received no external funding.

Data Availability Statement: The original contributions presented in the study are included in the article, further inquiries can be directed to the corresponding author.

Acknowledgments: The authors acknowledge TU Wien Bibliothek for financial support through its Open Access Funding Programme. The authors acknowledge that the paper is a part of the research project "PBS—Points-Beams-Structures" was funded by TU Wien in the "Innovative Idea" program.

Conflicts of Interest: The authors declare that the research was conducted in the absence of any commercial or financial relationships that could be construed as a potential conflict of interest.

References

1. Riggio, M.; Dilmaghani, M. Structural health monitoring of timber buildings: A literature survey. *Build. Res. Inf.* **2020**, *48*, 817–837. [CrossRef]
2. Cruz, H.; Yeomans, D.; Tsakanika, E.; Macchioni, N.; Jorissen, A.; Touza, M.; Mannucci, M.; Lourenço, P. Guidelines for On-Site Assessment of Historic Timber Structures. *Int. J. Archit. Herit.* **2015**, *9*, 277–289. [CrossRef]
3. Riggio, M.; D'Ayala, D.; Parisi, M.A.; Tardini, C. Assessment of heritage timber structures: Review of standards, guidelines and procedures. *J. Cult. Herit.* **2018**, *31*, 220–235. [CrossRef]
4. Pöchtrager, M.; Styhler-Aydın, G.; Hochreiner, G.; Özkan, T.; Döring-Williams, M.; Pfeifer, N. Bridging the gap. Digital models of historic roof structures for enhanced interdisciplinary research. *SCIRES* **2020**, *10*, 31. [CrossRef]
5. Perria, E.; Sieder, M. Six-Steps Process of Structural Assessment of Heritage Timber Structures: Definition Based on the State of the Art. *Buildings* **2020**, *10*, 109. [CrossRef]
6. Santos, D.; Sousa, H.S.; Cabaleiro, M.; Branco, J.M. HBIM Application in Historic Timber Structures: A Systematic Review. *Int. J. Archit. Herit.* **2023**, *17*, 1331–1347. [CrossRef]
7. Diara, F. HBIM Open Source: A Review. *ISPRS Int. J. Geo-Inf.* **2022**, *11*, 472. [CrossRef]
8. Barazzetti, L.; Banfi, F.; Brumana, R.; Gusmeroli, G.; Previtali, M.; Schiantarelli, G. Cloud-to-BIM-to-FEM: Structural simulation with accurate historic BIM from laser scans. *Simul. Model. Pract. Theory* **2015**, *57*, 71–87. [CrossRef]
9. Massafra, A.; Prati, D.; Predari, G.; Gulli, R. Wooden Truss Analysis, Preservation Strategies, and Digital Documentation through Parametric 3D Modeling and HBIM Workflow. *Sustainability* **2020**, *12*, 4975. [CrossRef]
10. Caciora, T.; Herman, G.V.; Ilies, A.; Baias, S.; Ilies, D.C.; Josan, I.; Hodor, N. The Use of Virtual Reality to Promote Sustainable Tourism: A Case Study of Wooden Churches Historical Monuments from Romania. *Remote Sens.* **2021**, *13*, 1758. [CrossRef]
11. Lemmens, M. Terrestrial Laser Scanning. In *Geo-Information: Technologies, Applications and the Environment*; Springer: Dordrecht, The Netherlands, 2011; pp. 101–121. [CrossRef]
12. DLUBAL RSTAB Software. Available online: https://www.dlubal.com/en/products/older-products/rstab-8/what-is-rstab (accessed on 15 July 2024).
13. Autodesk REVIT. Available online: https://www.autodesk.com/products/revit/features (accessed on 17 July 2024).
14. Rocha, G.; Mateus, L. A Survey of Scan-to-BIM Practices in the AEC Industry—A Quantitative Analysis. *ISPRS Int. J. Geo-Inf.* **2021**, *10*, 564. [CrossRef]
15. Branco, J.; Piazza, M.; Cruz, P. Structural analysis of two King-post timber trusses: Non-destructive evaluation and load-carrying tests. *Constr. Build. Mater.* **2010**, *24*, 371–383. [CrossRef]
16. Lourenço, P.; Sousa, H.; Brites, R.; Neves, L. In situ measured cross section geometry of old timber structures and its influence on structural safety. *Mater. Struct.* **2013**, *46*, 1193–1208. [CrossRef]
17. Gocál, J.; Sousa, H.; Brites, R.; Neves, L. Analysis of the Historical Truss in Village Bela Dulice. *Acta Sci. Pol. Form. Circumiectus* **2015**, *14*, 57–73. [CrossRef]
18. Cabaleiro, M.; Hermida, J.; Riveiro, B.; Caamano, J. Automated processing of dense points clouds to automatically determine deformations in highly irregular timber structures. *Constr. Build. Mater.* **2017**, *146*, 393–402. [CrossRef]
19. Serafini, A.; Riggio, M.; González-Longo, C. A database model for the analysis and assessment of historic timber roof structures. *Int. Wood Prod. J.* **2017**, *8*, 3–8. [CrossRef]
20. Cuartero, J.; Cabaleiro, M.; Sousa, H.; Branco, J. Tridimensional parametric model for prediction of structural safety of existing timber roofs using laser scanner and drilling resistance tests. *Eng. Struct.* **2019**, *185*, 58–67. [CrossRef]
21. Rocha, G.; Mateus, L.; Fernández, J.; Ferreira, V. A Scan-to-BIM Methodology Applied to Heritage Buildings. *Heritage* **2020**, *3*, 47–67. [CrossRef]
22. Ursini, A.; Grazzini, A.; Matrone, F.; Zerbinatti, M. From scan-to-BIM to a structural finite elements model of built heritage for dynamic simulation. *Autom. Constr.* **2022**, *142*, 104518. [CrossRef]
23. Sola-Caraballo, J.; Rincón-Calderón, J.; Rivera-Gómez, C.; López-Martínez, J.; Galán-Marín, C. On-Site Risk Assessment Methodology of Historic Timber Structures: The Case Study of Santa Cruz Church. *Buildings* **2022**, *12*, 935. [CrossRef]

24. Abreu, N.; Pinto, A.; Matos, A.; Pires, M. Procedural Point Cloud Modelling in Scan-to-BIM and Scan-vs-BIM Applications: A Review. *ISPRS Int. J. Geo-Inf.* **2023**, *12*, 260. [CrossRef]
25. Kirizsán, I.; Tudoreanu-Crișan, A. A Sustainable Approach to Reconstruction: Historical Roof Structure Interventions. *Sustainability* **2024**, *16*, 4325. [CrossRef]
26. Pepe, M.; Garofalo, A.R.; Costantino, D.; Tana, F.F.; Palumbo, D.; Alfio, V.S.; Spacone, E. From Point Cloud to BIM: A New Method Based on Efficient Point Cloud Simplification by Geometric Feature Analysis and Building Parametric Objects in Rhinoceros/Grasshopper Software. *Remote Sens.* **2024**, *16*, 1630. [CrossRef]
27. Massafra, A.; Prati, D.; Gulli, R. Reverse Engineering Workflows for the Structural Assessment of Historical Buildings. *Int. J. Archit. Herit.* **2024**, 1–22. [CrossRef]
28. *ISO 13822:2010*; Bases for Design of Structures—Assessment of Existing Structures. ISO: Geneva, Switzerland, 2010. Available online: https://www.iso.org/standard/46556.html (accessed on 25 July 2024).
29. *EN 16096*; Conservation of Cultural Heritage—Condition Survey and Report for Built Cultural Heritage. DIN: Berlin, Germany, 2012. Available online: https://www.austrian-standards.at/de/shop/din-en-16096-2012-10~p1966040 (accessed on 18 September 2024).
30. *EN 17121:2019*; Conservation of Cultural Heritage—Historic Timber Structures—Guidelines for the On-Site Assessment of Load-Bearing Timber Structures. Austrian Standards International: Vienna, Austria, 2019. Available online: https://www.austrian-standards.at/de/shop/onorm-en-17121-2019-11-01~p2499434 (accessed on 18 September 2024).
31. Niederwanger, G. Structural repair of damaged old bell towers based on dynamic measurements. *WIT Trans. Built Environ.* **1997**, *29*, 9. [CrossRef]
32. André, N.; Galimard, P.; Morlier, P. Structural assessment of a wooden bell-tower. *WIT Trans. Built Environ.* **2003**, *66*, 10. [CrossRef]
33. Ivorra, S.; Palomo, M.J.; Verdú, G.; Zasso, A. Dynamic Forces Produced by Swinging Bells. *Meccanica* **2006**, *41*, 47–62. [CrossRef]
34. Selvaggi, I.; Bitelli, G.; Serantoni, E.; Wieser, A. Point cloud dataset and fem for a complex geometry: The san luzi bell tower case study. *ISPRS Int. Arch. Photogramm. Remote Sens. Spat. Inf. Sci.* **2019**, *42*, 1047–1052. [CrossRef]
35. Quattrini, R.; Clementi, F.; Lucidi, A.; Giannetti, S.; Santoni, A. From TLS to FE Analysis: Points Cloud Exploitation for Structural Behaviour Definition. The San Ciraiaco's Bell Tower. *ISPRS* **2019**, *XLII-2/W15*, 957–964. [CrossRef]
36. Ghini, E.; Marra, M.; Palermo, M.; Gasparini, G.; Silvestri, S.; Azzara, R.M. Peak Displacement Response Induced by Bell-Swinging on the Masonry Tower in Castel San Pietro Terme, Bologna. In *Structural Analysis of Historical Constructions*; Endo, Y., Hanazato, T., Eds.; Springer: Cham, Switzerland, 2024; pp. 849–861. [CrossRef]
37. Grussenmeyer, P.; Landes, T.; Voegtle, T.; Ringle, K. Comparison Methods of Terrestrial Laser Scanning, Photogrammetry and Tacheometry Data for Recording of Cultural Heritage Buildings. *Int. Arch. Photogramm. Remote Sens. Spat. Inf. Sci.* **2008**, *37*, 213–218.
38. Wang, X.; Pan, H.; Guo, K.; Yang, X.; Luo, S. The evolution of LiDAR and its application in high precision measurement. *IOP Conf. Ser.* **2020**, *502*, 012008. [CrossRef]
39. Prati, D.; Zuppella, G.; Mochi, G.; Guardigli, L.; Gulli, R. Wooden Trusses Reconstruction and Analysis through Parametric 3D Modeling. *ISPRS Int. Arch. Photogramm. Remote Sens. Spat. Inf. Sci.* **2019**, *XLII-2/W9*, 623–629. [CrossRef]
40. Cotella, V.A. From 3D point clouds to HBIM: Application of Artificial Intelligence in Cultural Heritage. *Autom. Constr.* **2023**, *152*, 104936. [CrossRef]
41. Yang, S.; Hou, M.; Li, S. Three-Dimensional Point Cloud Semantic Segmentation for Cultural Heritage: A Comprehensive Review. *Remote Sens.* **2023**, *15*, 548. [CrossRef]
42. Musicco, A.; Buldo, M.; Rossi, N.; Tavolare, R.; Verdoscia, C. Enhancing 3D Modeling Efficiency via Semi-Automatic Point Cloud Segmentation and Multi-Lod Mesh Reconstruction. *SCIRES* **2024**, *14*, 233. [CrossRef]
43. Caciora, T.; Ilies, A.; Herman, G.V.; Berdenov, Z.; Safarov, B.; Bilalov, B.; Ilies, D.C.; Baias, S.; Hassan, T.H. Advanced Semi-Automatic Approach for Identifying Damaged Surfaces in Cultural Heritage Sites: Integrating UAVs, Photogrammetry, and 3D Data Analysis. *Remote Sens.* **2024**, *16*, 3061. [CrossRef]
44. Grasshopper Algorithmic Modeling for Rhino, Version 0.9.0076. Robert Mcneel & Associates. Available online: https://www.grasshopper3d.com/group/element?overrideMobileRedirect=1 (accessed on 5 August 2024).
45. Yang, X.; Koehl, M.; Grussenmeyer, P. Reality-Based Data by Revit Api Development. In *Latest Developments in Reality-Based 3D Surveying*; MDPI: Basel, Switzerland, 2018. [CrossRef]
46. Pöchtrager, M.; Styhler-Aydin, G.; Döring-Williams, M.; Pfeifer, N. Digital reconstruction of historic roof structures: Developing a workflow for a highly automated analysis. *Virtual Archaeol. Rev.* **2018**, *9*, 21–33. [CrossRef]
47. Murtiyoso, A.; Grussenmeyer, P. Virtual Disassembling of Historical Edifices: Experiments and Assessments of an Automatic Approach for Classifying Multi-Scalar Point Clouds into Architectural Elements. *Sensors* **2020**, *20*, 2161. [CrossRef]
48. Özkan, T.; Pfeifer, N.; Styhler-Aydin, G.; Hochreiner, G.; Herbig, U.; Döring-Williams, M. Historic Timber Roof Structure Reconstruction through Automated Analysis of Point Clouds. *J. Imaging* **2022**, *8*, 10. [CrossRef]

49. Özkan, T.; Pfeifer, N.; Styhler-Aydin, G.; Hochreiner, G.; Herbig, U.; Döring-Williams, M. Structural Assessment of Historic Timber Roofs by Improved Automation of Point Cloud Processing. In Proceedings of the International Conference on Structural Health Assessment of Timber Structures, Prague, Czech Republic, 7–9 September 2022; pp. 119–124.
50. Selman, Z.; Musto, J.; Kobbelt, L. Scan2FEM: From Point Clouds to Structured 3D Models Suitable for Simulation. In *Eurographics Workshop on Graphics and Cultural Heritage*; Ponchio, F., Pintus, R., Eds.; The Eurographics Association: Eindhoven, The Netherlands, 2022. [CrossRef]
51. Özkan, T.; Pfeifer, N.; Hochreiner, G. Automatic completion of geometric models from point clouds for analyzing historic timber roof structures. *Front. Built Environ.* **2024**, *10*, 1368918. [CrossRef]
52. St. Michaeler Church. St. Michaeler Church. 2024. Available online: https://www.michaelerkirche.at/en/ (accessed on 25 October 2024).
53. Federal Monuments Authority of Austria. Federal Monuments Authority of Austria Website. 2024. Available online: https://www.bda.gv.at (accessed on 25 October 2024).
54. Riegl VZ-400i Terrestrial Laser Scanner. Available online: https://www.riegl.com/nc/products/terrestrial-scanning/produktdetail/product/scanner/48/ (accessed on 15 July 2024).
55. EKG-Baukultur. EKG-Baukultur. 2024. Available online: https://ekg-baukultur.com/ (accessed on 25 October 2024).
56. Laser (LAS) File Format. Available online: https://www.asprs.org/divisions-committees/lidar-division/laser-las-file-format-exchange-activities (accessed on 6 August 2024).
57. RiScanPRO 2.15. Available online: https://www.riegl.com/products/software-packages/riscan-pro/ (accessed on 15 July 2024).
58. Pfeifer, N.; Mandlburger, G.; Otepka, J.; Karel, W. OPALS—A framework for Airborne Laser Scanning data analysis. *Comput. Environ. Urban Syst.* **2014**, *45*, 125–136. [CrossRef]
59. STEP, Industrial Automation Systems, and Integration—Product Data Representation and Exchange (Version ISO 10303-21:2016). Available online: https://www.loc.gov/preservation/digital/formats/fdd/fdd000448.shtml (accessed on 15 July 2024).
60. Autodesk ReCap Pro. Available online: https://www.autodesk.com/products/recap/overview?term=1-YEAR&tab=subscription (accessed on 17 July 2024).
61. Katz, S.; Tal, A.; Basri, R. Direct visibility of point sets. *Acm Trans. Graph.* **2007**, *26*, 24-es. [CrossRef]
62. Gambotto, J.P. A new approach to combining region growing and edge detection. *Pattern Recognit. Lett.* **1993**, *14*, 869–875. [CrossRef]
63. Jolliffe, I. Principal Component Analysis. In *International Encyclopedia of Statistical Science*; Lovric, M., Ed.; Springer: Berlin/Heidelberg, Germany, 2011; pp. 1094–1096. [CrossRef]
64. Fischler, M.; Bolles, R. Random sample consensus: A paradigm for model fitting with applications to image analysis and automated cartography. *Commun. ACM* **1981**, *24*, 381–395. [CrossRef]
65. Dai, J.S. Euler–Rodrigues formula variations, quaternion conjugation and intrinsic connections. *Mech. Mach. Theory* **2015**, *92*, 144–152. [CrossRef]
66. Kazhdan, M.; Bolitho, M.; Hoppe, H. Poisson surface reconstruction. In Proceedings of the Fourth Eurographics Symposium on Geometry Processing, Cagliari, Italy, 26–28 June 2006; pp. 61–70.
67. Besl, P.; McKay, N.D. A method for registration of 3-D shapes. *IEEE Trans. Pattern Anal. Mach. Intell.* **1992**, *14*, 239–256. [CrossRef]
68. Shortest Line Connector Between Line Segments in 3D. Available online: https://www.geometrictools.com/GTE/Mathematics/DistSegmentSegment.h (accessed on 18 July 2024).
69. IFC, Industry Foundation Classes (IFC), IFC Data File Formats. Available online: https://docs.fileformat.com/cad/ifc/ (accessed on 15 July 2024).
70. CloudCompare Version 2.11.3. Available online: https://www.cloudcompare.org (accessed on 10 July 2024).
71. *ISO 19650-1:2018*; Organization and Digitization of Information About Buildings and Civil Engineering Works, Including Building INFORMATION Modelling (BIM)—Information Management Using Building Information Modelling Part 1: Concepts and Principles. ISO: Geneva, Switzerland, 2018. Available online: https://www.iso.org/standard/68078.html (accessed on 19 November 2024).